Determining the Angle to Produce Maximum Downforce on the Wing of an Acura RSX Type S

Nathan Correia
1615561

ABSTRACT

Our group will analyze the rear wing of an Acura RSX and optimize the angle needed for maximum downforce. By maximizing the downforce, the grip of the car will be increased allowing it to go faster around corners. This will be done by altering the angle of attack of the model in increments of 15°.

The simulation will analyze using 2-D, turbulent, steady-state flow and the following parameters:

- Inlet velocity: 1.9m/s
- Re: 3800
- Chord length: 30mm
- No slip at wing
- Free slip at walls

The simulation found 25° to be the optimal angle as it generated the most downforce and was the second most efficient angle with respect to drag. 15° could also be used as it was the most efficient, but had considerably less downforce than 25°.

INTRODUCTION

Optimizing the downforce generated by a spoiler can drastically improve the performance of a car that is traveling and performing turns at high speeds. In this study, the aim is to find the angle of attack of the rear spoiler wing that will maximize the lift in the negative Y direction generated when air flows around the wing. The study involves altering the angle of attack of the model within the simulation, starting at 0° and increasing in increments of 15°. The results are highly applicable in developing a more optimized design for the rear wing of the Acura RSX, and other similar car models. This report will also discuss the limitations and accuracy of the simulation when compared to the simplified analytical solution or experiments conducted in a wind tunnel.

Computational Fluid Dynamics (CFD) is broadly defined as the use of computational software in order to apply mathematical equations to describe fluid flow. For the case of turbulent flow, these mathematical equations are called the RANS (Reynolds Averaged Naiver Stokes) model, which are simplified and decomposed variations of the Navier-Stokes Equations specifically applied for turbulent flows. The application of CFD and RANS modeling is especially useful in situations where it is difficult to obtain analytical solutions. Due to the turbulent nature and the presence of large wakes behind the model of the wing, an analytical solution is impossible to obtain, and is a perfect application for CFD. In addition, by using CFD simulations as opposed to physical experiments such as a wind tunnel, a lot of resources can be saved. The simulation discussed in this report heavily relies on the use of RANS modeling to investigate the flow behavior around the wing, and thus optimize the angle of attack to maximize downforce. The study also looks at different models, their known challenges and benefits, and their potential relevance to the case study in question.

The 4 most common turbulence models that were considered for the simulation are the standard k-ε model, the RNG k-ε model, the standard k-ω model and the shear stress transport model. Each of these models comes with its own strengths and weaknesses, but ultimately, the k-ε turbulence model was chosen due to its robustness and its ability to accurately model flows away from a wall. The other three models are generally more accurate for predicting flows near walls, however, this was not required for our simulation as the critical flow region was behind and below the wing. In addition, these other models, while more accurate, are also more expensive and require more computational resources.

METHODOLOGY

The problem addressed in this report is to optimize the angle of attack of the rear wing of an Acura RSX in order to achieve maximum downforce. This optimization will be carried out through a series of 2D simulations of the airflow around the wing, using ANSYS CFX. The wing was made in SOLIDWORKS and imported as an .IGS file.

Firstly, in order to define and simplify the problem, the following assumptions were made:

- Steady-state flow
- Incompressible flow
- Turbulent flow
- Two-dimensional flow

The implication of Steady-state flow assumption is that transient effects are not captured in the simulation, while the implication of the incompressible flow assumption is that compressibility effects are not captured. For the turbulent flow assumption, the implication is that we need to use a turbulence solver, and that the grid must be fine enough to capture eddies that are formed as a result of this turbulence. Finally, for the two-dimensional flow assumption, the implication is that three-dimensional effects like vortex shedding may not be

captured to the full extent that they would normally occur in real world simulations.

Using these assumptions, the Navier-Stokes equations, and the Continuity equation, the final governing equations can be simplified to:

$$\textbf{x-dir}: \quad \rho\left(u\frac{\partial u}{\partial x} + u\frac{\partial u}{\partial y}\right) = -\frac{\partial P}{\partial x} + \mu\left(\frac{\partial^2 u}{\partial x^2} + \frac{\partial^2 u}{\partial y^2}\right)$$

$$\textbf{y-dir}: \quad \rho\left(v\frac{\partial v}{\partial x} + v\frac{\partial v}{\partial y}\right) = -\frac{\partial P}{\partial y} + \mu\left(\frac{\partial^2 v}{\partial x^2} + \frac{\partial^2 v}{\partial y^2}\right)$$

These equations are then solved within the ANSYS software itself to create a solution.

The next step in our project was to determine a domain size. Our initial domain had dimensions of 0.55C from the inlet to the wing, 0.4C from the wing to the simulation walls, and 1.4C from the wing to the outlet, where C is the chord length of 30mm. This size was, however, much too small and did not accurately capture the flow characteristics. The domain size we ended up choosing after doing domain independence had a domain size of 0.55C from the inlet to the wing, 0.8C from the wing to the simulation walls, and 2.2C from the wing to the outlet.This domain and the flow conditions around it can be seen below in Figure 1.

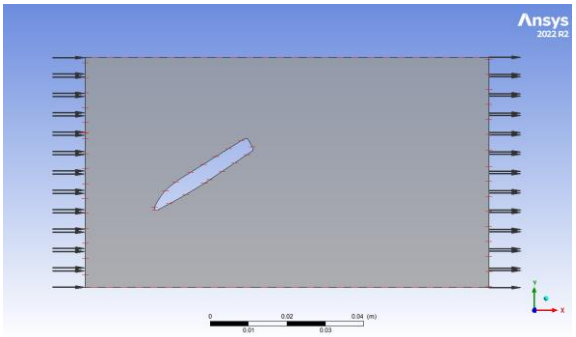

Figure 1: Screenshot of the computational domain

The following Boundary conditions were then used to model the flow:

- No slip condition at the wings surface
- Free slip condition at walls
- Dirichlet boundary condition at the inlet
- Free stream velocity of 1.9m/s
- Neumman boundary condition at the outlet
- A relative pressure at the outlet of 0 Pa
- Symmetry boundary condition

As for the numerical scheme used to perform the simulations, the Central differencing scheme was chosen as it has greater accuracy than alternatives such as the backwind and upwind differencing schemes. It also reaches mesh and domain independence faster, allowing for a lower overall computational cost and less time required waiting for simulations to converge.

The turbulence solver used for our simulations was the k-ε model. In short, k-ε turbulence modeling is a popular two-equation model used to simulate turbulent flow in computational fluid dynamics (CFD). The model consists of two transport equations, one for the turbulent kinetic energy (k) and the other for the turbulent dissipation rate (ε). The turbulent kinetic energy equation describes how much energy is stored in the turbulent eddies and how much is transferred between them and the mean flow. The turbulent dissipation rate equation describes the rate at which turbulent kinetic energy is dissipated into heat by viscous forces. Constants in the k-ε model include the $C_{1\varepsilon}$ and $C_{2\varepsilon}$ constants, which are used to model the dissipation rate equation, and the $\boldsymbol{\sigma}_k$ and $\boldsymbol{\sigma}_\varepsilon$ constants, which are used to model the turbulent diffusion terms in the equation, as well as the C_μ constant which is used to determine eddy viscosity. These constants are all set within the ANSYS software.

Next, for the initial conditions in the simulation, we used an inlet velocity of 1.9 m/s in order to achieve a Reynolds number that would result in turbulent flow. The turbulence intensity was set at medium (5%) to mimic the conditions of air coming down from the roof of the car. The relative pressure of the outlet was also set at 0 Pa.

For convergence within the simulations, we used residuals set at 1.0e-5, and then monitored properties such as pressure and vorticity at certain points. If the simulations were taking too long, we set the maximum iterations to 100 in order to reduce time and expenses. When the monitored properties flattened out, we could consider the solutions as converged. All of our simulations satisfied at least one of the above criteria.

The properties of the chosen fluid, which was air, were taken at SATP.

- Temperature, T = 25°C
- Pressure, P = 1 atm
- Density, $\rho = 1.184$ kg/m^3
- Dynamic viscosity, $\mu = 1.849\text{x}10^{-5}$ kg/ms

The properties are crucial in setting up the fluid simulation and are indicative of the behavior of air under the given conditions.

VERIFICATION

The meshing process was a critical component of the simulations, as it directly impacted the accuracy and reliability of our results. To create the final mesh shown in Figure 2, we took into account a multitude of factors, including the size of the domain, the element size, and the transition ratio of the inflation layer. The domain size was carefully chosen to ensure that we captured the entirety of the flow field around the wing, while also avoiding any unnecessary computational overhead.

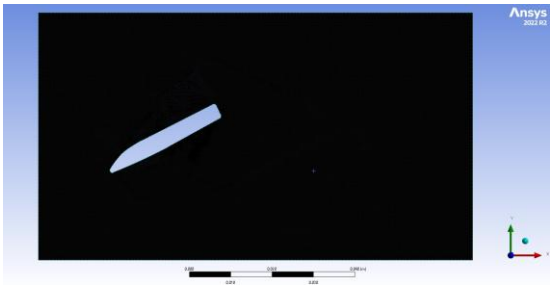

Figure 2: Screenshot of Final Mesh

The element size of 1x10-4m was selected based on our previous experience and mesh independence study and was determined to be the optimal size to balance computational resources and accuracy. To accurately capture the boundary layer flow, an inflation layer was added around the wing's surface. This layer had a transition ratio of 0.25, meaning that the mesh density increased gradually from the outer boundary to the inner boundary.

The growth rate of the inflation layer was set at 1.2 to ensure that the mesh was dense enough to capture the small-scale flow features that occur near the wing's surface. However, we did not want to make the mesh too fine away from the boundary layer, as we did not expect the flow to have significant changes there. The rest of the domain was therefore meshed with a fairly fine grid that allowed us to capture the effects of the wing on the stream, while avoiding unnecessary computational costs.

The element size of our final mesh was $1x10^{-4}$m. Results started converging after our mesh was refined past the point of $1.25x10^{-4}$m. After analyzing a refined mesh at $8x10^{-5}$m and seeing little change, we deemed the mesh of size $1x10^{-4}$m to be refined enough. This can be seen in Figure 3. The key characteristics of the pressure contour are similar between the two and due to time and computational restrictions, we chose not to use the finest mesh.

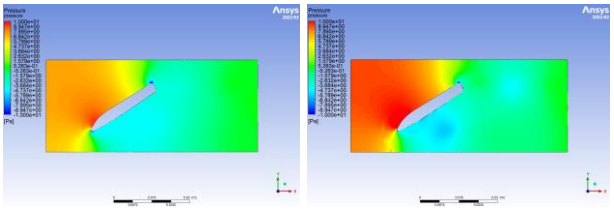

Figure 3: Left to right, 1.0e-4m and 8.0e-5m element sizes

Our final mesh had a domain of 0.55C from inlet to object, 0.8C from the object to the simulation walls, and 2.05C from the object to the outlet, where C is the chord length of 30mm. The standard domain size of 5C to the inlet, 5C to walls and 25C to the outlet was not used due to computational and time limitations. Our simulation results did converge as our domain size increased, the largest domain size considered being 0.88C to the inlet, 1.12C to walls and 2.88C. From Figure 4, seeing as the increasing domain size did not affect the results significantly, we opted for a less time consuming domain size that still yielded accurate results.

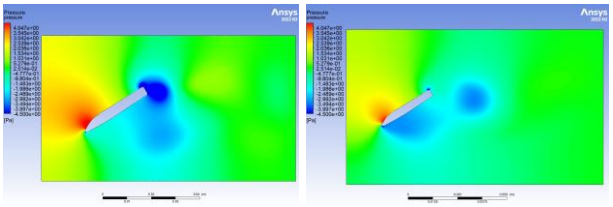

Figure 4: Left to right, domain size used and large domain size

The minimum and maximum y^+ values in our final mesh range from 0.1 to 0.55. Being that this is less than 3.0, the quality of our grid is fine enough near the surface of the wing and can be expected to accurately model the boundary layer around the wing with little error.

RESULTS & DISCUSSION

The turbulent and laminar cases were both initially run to determine if the flow around the wing was truly turbulent. Monitor points were also placed in various locations on and around the wing to measure the values of Turbulent Kinetic Energy. Below is the plot of turbulent kinetic energy for the largest angle:

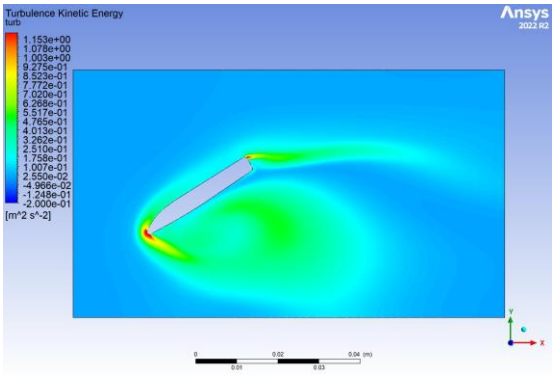

Figure 5: Plot of Turbulent Kinetic Energy (30°)

We can see that the values are highest near the front and the rear of the wing. By taking the maximum value of Turbulent Kinetic Energy on the plot above and dividing it by the free stream velocity squared, which is 1.9 m/s, we can find the turbulence intensity, I:

$$I = \frac{k}{u^2} = 0.32$$

This value is well above the laminar cut off of 0.1, proving that there are turbulent features within the flow and that it needs to be solved using a turbulent solver. Doing the same calculation downstream from the flow, we get values varying from 0.14 - 0.25, further providing justification for the need for turbulence modeling.

Once this was confirmed, we were able to use the turbulent solver for the rest of the models. For this project, we tested the effects of changing the angle of attack on the coefficients of lift and drag. After running all of the simulations, we found that the two angles that created the most lift were 15° and 25°, of whose streamlines are plotted below in Figures 6 and 7.

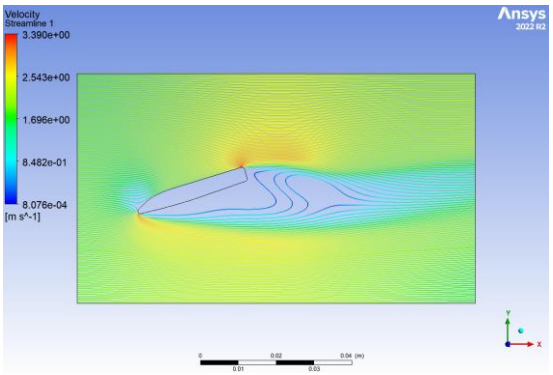

Figure 6: Streamline plot of Velocity (15°)

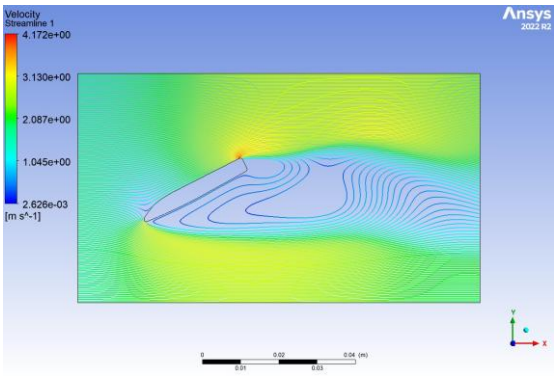

Figure 7: Streamline Plot of Velocity (25°)

After the mesh analysis was all run, we were able to calculate the order of accuracy. This was determined from the number of elements from each mesh size, as well as the calculated lift from each simulation. The table with all of the obtained values is shown below:

Table 1. Values from Mesh Independence.

Mesh	**Elements**	***Lift (N)***
#1	45842	-7.36e-5
#2	179545	-8.36e-5
#3	286881	-8.60e-5

Taking these values and calculating r_{12} and r_{23}, which were necessary because our element size did not increase incrementally, we were then able to get the order of accuracy. The calculation with all the values is shown below:

$$P = \frac{log((\frac{1.264-1}{1.979-1})(\frac{-8.36e-5-(-7.36e-5)}{-8.60e-5-(-8.36e-5)}))}{log(1.979)} = 0.140$$

This value is smaller than the theoretical value of 2.00, but is expected due to the hardware and time restraints preventing us from pursuing further grid testing.

The plot detailing the lift force created by each angle has also been plotted below in Figure 8.

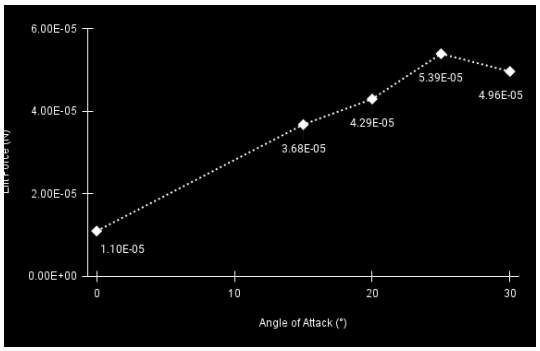

Figure 8: Plot of Lift Force as a function of the Angle of Attack

We can see that as the angle of attack increases, the lift force does as well, up to an angle between 25° and 30°, when it starts to drop.

We also plotted the Efficiency of the wing, defined as the ratio of lift to drag, to see if 25° still was the best decision. As can be seen in Figure 9, 15° has the highest ratio, with values decreasing afterwards. However, because we are simply looking for lift alone, 25° is the best choice.

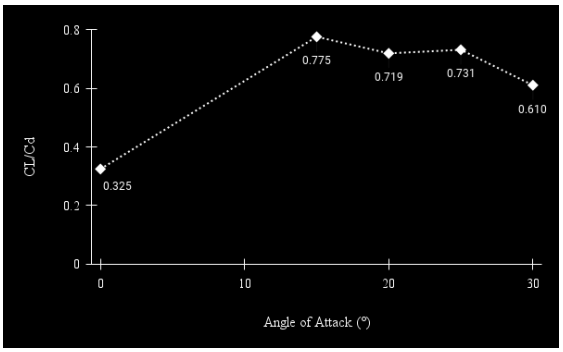

Figure 9: Efficiency of Wing as a function of the Angle of Attack

CONCLUSION

In conclusion, this study aimed to find the optimal angle of attack for the rear wing of an Acura RSX Type S to maximize downforce using ANSYS CFX. The simulation used a k-ε turbulence solver to accurately model flows away from the wall and converge quickly.

By altering the angle of attack of the model in increments of 15°, and refining in increments of 5°, the simulation found that 25° generated the most downforce and was the second most efficient angle with respect to drag. 15° produced a higher ratio of lift to drag, but was ultimately not chosen as the loss of downforce was too significant to justify the small gain of efficiency.

REFERENCES

1. CFD Ninja. "Ansys Meshing Sizing 2." [Online]. Available: https://cfd.ninja/ansys-meshing/ansys-meshing-sizing-2/ [Accessed: Apr. 1, 2023].

2. Ideal Simulations. "CFD Computational Domain." [Online]. Available: https://www.idealsimulations.com/resources/cfd-computational-domain/ [Accessed: Apr. 4, 2023].

3. Ideal Simulations. "Turbulence Models in CFD." [Online]. Available: https://www.idealsimulations.com/resources/turbulence-models-in-cfd/ [Accessed: Apr. 5, 2023].

4. J.A. Bakker, "Introduction to RANS turbulence modeling," Technical report, Institute for Computational Mechanics in Engineering, Universidade de São Paulo, São Paulo, Brazil, 2010. [Online]. Available: https://sites.icmc.usp.br/gustavo.buscaglia/cursos/mfc_undergrad1/bakker_10-rans.pdf [Accessed: Apr. 9, 2023].